Towards a truly biomimetic olfactory microsystem: an artificial olfactory mucosa

J.A. Covington, J.W. Gardner, A. Hamilton, T.C. Pearce and S.L. Tan

Abstract: Today, the capability of the human olfactory system is still, in many ways, superior to that of the electronic nose. Although electronic noses are often compared with their biological counterpart, they neither mimic its neural architecture nor achieve its discriminating performance. Experimental studies on the mammalian olfactory system suggest that the nasal cavity, comprising of the mucous layer and the olfactory epithelium, performs a degree of chromatographic separation of complex mixtures. Thus receptor cells distributed beneath the mucous layer provide both spatial and temporal chemosensory information. Here we report on the development of an artificial olfactory microsystem that replicates this basic structure. This contains an integrated channel to emulate the nasal cavity and coated with a polymer to mimic the partitioning mucous layer, which is positioned directly over a sensor array. Our system employs an 80 element chemoresistive microsensor array with carbon black/polymer odour-sensitive films combined with a microfluidic package fabricated by micro-stereolithography. Results show that this biomimetic system generates both spatial and temporal odorant signals, with a temporal chemical retention period of up to 170 s. Data analysis has revealed improvements in its ability to discriminate between two simple odours and a set of complex odours. We believe such emulation of the olfactory system can lead to improved odour discrimination within the field of electronic noses.

1 Introduction

The sense of smell is the least understood of our five human senses. Olfaction itself is of great importance to many species and is used for navigation, food sourcing and sexual reproduction [1]. The sense of smell has been extensively studied over the past 40 years, although it is only relatively recently that the underlying sensory mechanisms are becoming better understood [2]. Artificial olfaction has been with us since the early 1980s, although the term 'electronic nose', or e-nose, was only defined as recently as 1994 by Gardner and Bartlett. Such systems try not to identify specific chemicals within a complex odour, for example coffee is made up of over 1000 headspace compounds, but more to classify the type of aroma. E-noses typically combine an array of chemical sensors with partially overlapping sensitivities. Hence each sensor responds to a class of chemical components within an odour, for example ketones. Identification is possible due to the differences between complex odours in the concentration and mixture of chemical components. Consequently the sensors produce a response profile, or chemical fingerprint, which can be matched to a specific odour. The identification process is usually performed with some form of statistically based multivariate method or non-parametric neural network. Such systems are used regularly in, for example, environmental testing and food quality [3].

Even with the success of many e-nose systems their performance, in terms of odour sensitivity and selectivity, still lags behind that of the human olfactory system. It is generally believed that this is due to the lower complexity of e-noses when compared with their biological counterparts. For example the human olfactory system contains some 100 million olfactory receptors with approximately 350 different types of receptor binding proteins, distributed along the olfactory epithelium (the lining of the nose and part of the olfactory mucosa). In contrast e-nose systems typically have $\leq$32 chemical sensors in a basic chamber. Many studies of the biological system have shown that the mucus layer coating of the nasal epithelium has partitioning type properties. An effect comparable to a gas chromatograph (GC). It is believed that this partitioning process contributes to the coding of olfactory information [4, 5]. In both systems, a retentive coating on the sides of the column, or nasal cavity, delays the transport of certain compounds within the odour as it traverses along the column. This delay depends on the affinity (or partitioning) of the compound with the retentive coating. In a GC system a single sensor is used to detect the separated odour components as they elude from the end of the column. For the biological system, receptor cells distributed underneath this mucous coating have been shown to generate both spatial (response magnitude) and temporal (time delayed) signals [6]. It is believed that this biological response to an odour stimulus results in a spatio-temporal map being formed for that odour, which is passed on to the olfactory bulb. Researchers have hypothesised that these signals could, conceivably, be an important principle that enhances our ability to discriminate between similar odours [7, 8]. Here our aim is to model and fabricate a microsystem that

doi:10.1049/iet-nbt:20060015

Paper first received 3rd August and in revised form 21st December 2006

J.A. Covington, J.W. Gardner and S.L. Tan are with the School of Engineering, University of Warwick, Coventry CV4 7AL, UK

A. Hamilton is with the School of Electronic and Electrical Engineering, University of Edinburgh, Mayfield Road, Edinburgh EH9 3JL, UK

T.C. Pearce is with the Department of Engineering, University of Leicester, University Road, Leicester LE1 7RH, UK

E-mail: j.a.covington@warwick.ac.uk

mimics more closely the human olfactory mucosa. We believe that such an approach will offer faster analysis times over traditional GC systems and improved discrimination over current electronic technology. By doing so we aim to improve upon existing e-nose systems by developing a new enabling technology for low cost portable e-nose systems.

2 Artifical olfactory mucosa simulations

Before fabrication, numerous simulations were carried out to identify the optimum working conditions for promoting odour separation. A finite element model was created using FEMLAB (Ver. 2.3, Comsol, UK) software to simulate the odour transport and retentive behaviour of our system. This could not be achieved using a commercial GC simulation package because our model needs to include the sensors located at various points along the channel. In order to ensure the accuracy of our model, a commercial GC column was first modelled and the analytical solution was found to be accurate ($<3\%$ error in retention time and $<9\%$ error in separation factor).

A section of our artificial olfactory mucosa is shown in Fig. 1. The simulation model comprised of a 2.4 m × 0.5 mm × 0.5 mm channel with 40 sensors (five different sensing materials) distributed along it. These sensors were placed into 8 groups of 5, with each group containing one sensor of each sensing material. The sensors in a block were separated by 20 mm and each block was separated by 150, 250, 280, 250, 280, 250, and 150 mm. The sensors have been designated so that sensor S1 was located at 10 mm and sensor S40 was at 2260 mm along the channel. The stationary phase used in the simulations was the commercial polymer Parylene C (poly monochloro-para-xylene C).

Results from the simulations showed that the optimum velocity for column efficiency was 7 cm/s, although the effect of increasing flow velocity was found to be marginal on column efficiency. This velocity gives the best compromise between the unwanted broadening effect (the faster the flow the less the odour pulse front diffuses while traversing down the channel) and the desirable retention effect (the slower the flow rate the higher the separation of components in the odour).

On completion of these initial calculations, the outputs at the sensor locations along the channel were coupled with the sensor responses to model the complete system. To produce a more reliable simulation, previously fabricated sensors were tested at different velocities (0–1600 cm/s) to pulses of ethanol and toluene vapour in air (test temperature 30 ± 2 °C, humidity 40 ± 5% r.h., sensor resistance typically 2–8 kΩ). This was done in a micro-chamber

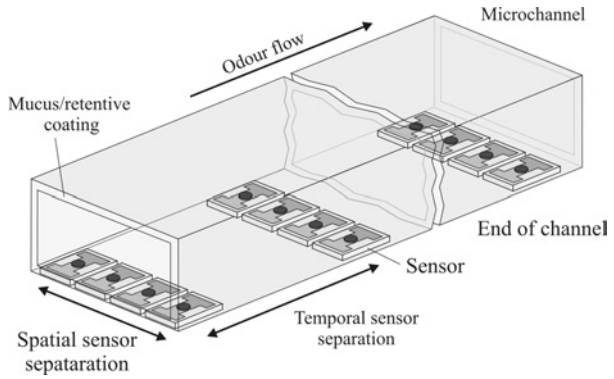

Fig. 1 *Section of the artificial olfactory mucosa*

system to help create boundary conditions for laminar plug flow. Further details covering the fabrication and test results of these sensors can be found in [9]. The sensors employed polymer/carbon black composite materials as the odour sensitive element. Here a non-conductive polymer is combined with 80–50 nm diameter carbon nanospheres that endow good electrical conduction to the resultant mix [10]. The sensing materials were chosen due to their rapid (ms) response time, ease of deposition, room temperature operation and the wide variety of available polymers. Five different sensor materials were tested for use in our simulations (poly(styrene-co-butadiene) (PSB), poly(ethylene glycol) (PEG), poly(caprolactone) (PCL), poly(ethylene-co-vinyl acetate) (PEVA) and poly(vinyl pyrrolidone) (PVPD), with a 20% loading by weight of carbon black). More details on the sensor materials deposition are given in Section 3.1. The sensor responses were modelled using a simple first-order exponential model for both the 'on' and 'off' transients, given by

$$R = R_{ON}(1 - e^{-\tau_{ON}t}) \quad (1)$$

$$R = R_{OFF}e^{-\tau_{OFF}t} \quad (2)$$

where R is the sensor resistance, R_{ON} is the response magnitude, τ_{ON} is the response time coefficient, R_{OFF} is the decay magnitude and τ_{OFF} is the decay time coefficient. The measured parameters from the tests are given in Table 1.

Fig. 2*a* shows profile information for a 5 s ethanol pulse (flow rate of 50 cm/s) at 5 points along the channel. As can be seen, the ethanol vapour pulse broadens out as it transverses along the channel due to the diffusion effect and the retention effect of the stationary phase coating (thickness 10 μm). Fig. 2*b* shows the sensor responses at different points along the channel. The difference in retention time between sensors for each odour produces temporal signals. As different types of sensors are being used, the highly similar profiles (slowly broaden pulse) will produce very different sensor responses.

These simulations show that it should be possible to create a system in which both spatial and temporal informations can be acquired, similar to the human olfactory mucosa.

Table 1: Experimental results of sensor responses to ethanol and toluene vapours in air (simple polar and non-polar odours) fitted to a first-order exponential dynamic model

Sensor type	R_{ON}	τ_{ON}	R^2
Ethanol			
PSB	0.5346	0.3568	0.8638
PEVA	2.6793	0.7229	0.9626
PEG	35.1677	0.0630	0.9945
PCL	0.8580	0.103	0.9477
PVPH	2.1748	0.1887	0.9928
Toluene			
PSB	3.3282	0.4062	0.9902
PEVA	20.9653	0.5349	0.9870
PEG	32.5009	0.1445	0.9948
PCL	7.7427	0.0807	0.9964
PVPH	2.1630	0.1881	0.9950

R^2 is the square of the correlation coefficient

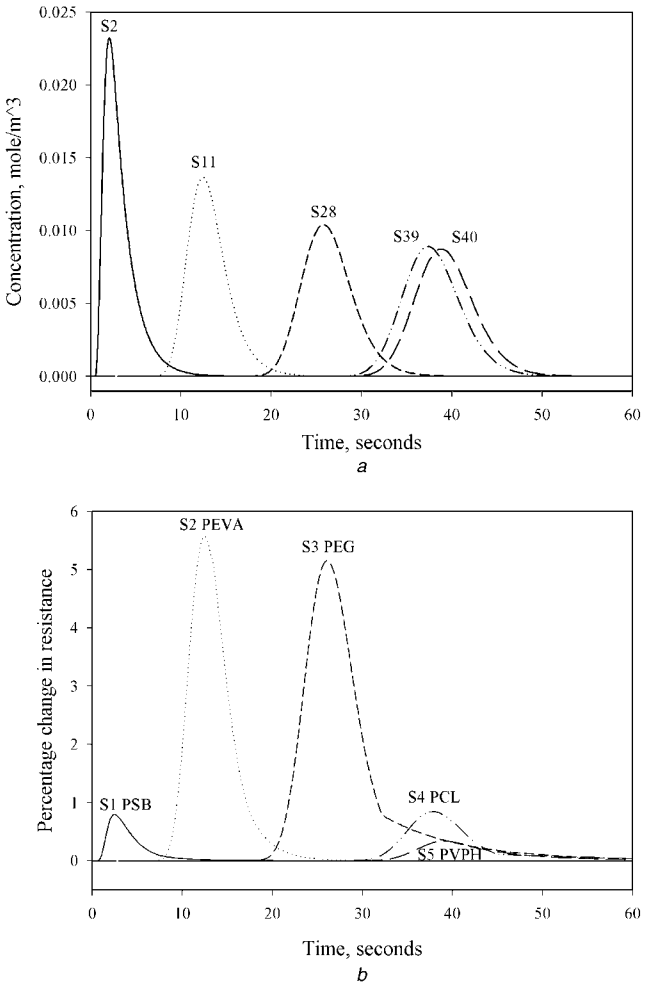

Fig. 2 *Simulation of ethanol pulse profiles and sensor responses at different points along the channel*

a Simulation of ethanol pulse profiles along the channel
b Sensor responses to ethanol vapour in air at the same locations as *a* along the channel for different sensing materials

3 Artifical olfactory mucosa microsystem

On completion of the simulations, a microsystem was fabricated to further investigate these spatio–temporal signals. The microsystem comprised of a silicon-based microsensor array and a microfluidic package. This final microsystem was fabricated at a scale that could be used for portable e-nose systems, hence making it more applicable to real world applications. Details of these system components are given in the following sections.

3.1 Silicon-based microsensor array and sensing coating

The microsensor array was fabricated using standard silicon processing techniques and then coated with polymer composite sensing materials. Each silicon die was 10 mm × 10 mm in size and contained 80 microsensors. Each sensor was formed by a pair of thin gold electrodes (20 nm chrome/200 nm gold, deposited by evaporation) deposited on top of a SiO_2 passivation layer (450 nm, grown by thermal oxidation). The sensor elements were nominally 200 μm × 200 μm in size, with an electrode gap of 20 μm and an aspect ratio of 10. The device was passivated using an epoxy coating SU-8-10 (10 μm thick layer, Microchem, UK) with openings for deposition of sensing materials and bonding. Owing to the simplicity of the array, only one metal layer was required for electrical contacts. Five different polymer composite recipes were used to produce the sensing materials, as given in Table 2.

Table 2: Sensing materials and solvents used to coat the microsensor array

Polymer	carbon black, g	solvent
poly stylene-co-butadiene (PSB), 0.7 g	0.175	toluene, 20 ml
poly ethylene-co-vinyl acetate (PEVA), 1.2 g	0.3	toluene, 20 ml
poly ethylene glycol (PEG), 1.2 g	0.3	ethanol, 20 ml
poly caprolactone (PCL), 1.2 g	0.3	toluene, 20 ml
poly 4-vinyl phenol (PVPH), 1.2 g	0.3	ethanol, 20 ml

The polymers were supplied by Sigma Aldrich (UK) and the carbon black (Black Pearls 2000) was supplied by Cabot Corporation (USA). The polymers were either in powder form or small crystals whereas the carbon black was supplied as nanospheres with diameters of typically 80–50 nm. The polymers were first dissolved in their respective solvent overnight, with the aid of a magnetic stirrer and at an elevated temperature (50 °C). Next, carbon black was added and the mixture sonicated for 10 min using a flask shaker (Griffin and George, UK). The mixture was then deposited onto the sensor electrodes using an airbrush (HP-BC Iwata, Japan) controlled by a micro-spraying system (RS precision liquid dispenser, UK). A beryllium copper mask was etched with 300 μm diameter holes, using standard photolithography techniques, to aid deposition of the sensing material and reduce the possibility of cross contamination. The sensor electrodes were aligned to the mask using an X–Y stage before deposition occurred. The airbrush was held 10–15 cm away from the mask and several passes were sprayed depending on the desired thickness (or resistance). This gave a circular coating of typically 300 ± 50 μm in diameter and 20 ± 5 μm thick. The electrical resistances of the sensors were controlled through the deposition process to a value of 2–8 kΩ. After coating, the sensor array was mounted in a 256 pin PGA package (Spectrum Semiconductor, USA). Fig. 3 shows a photograph of a fabricated microsensor array which has been coated with sensing materials. Further details on the sensor array can be found in [12].

3.2 Microfluidic package

The microfluidic package was fabricated using a modified Envisiontec perfactory mini micro-stereolithography (MSL) machine. Micro-stereolithography (MSL) is a similar process to stereolithography, which is used extensively for rapid prototyping. In an MSL system, a 3D CAD model of the object is first created, this CAD model is then sliced horizontally into a series of 2D images that represent multiple cross-sections of the 3D object. These layers are translated into appropriate control and positioning co-ordinates and are cured layer by layer (cross-section by cross-section) into a photocurable resin. After each layer has been cured into the resin, the object is moved vertically to allow an uncured layer of resin to cover the previously cured layer. The perfectory MSL system employs projection-based (dynamic masking) technology. The hardware consists of a visible light source, a dynamic mask modulator (implemented using a digital micro-mirror device, DMD), focusing optics, a resin tray and a Z-stage

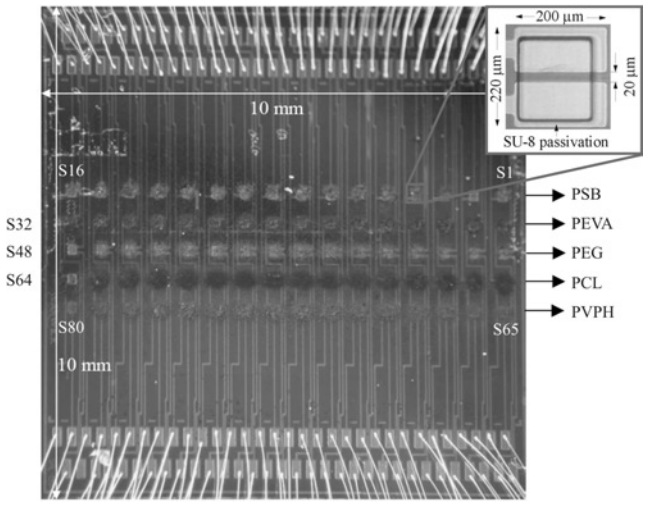

Fig. 3 *Photograph of a fabricated microsensor array with sensing coating*

Sensor materials have been labelled and sensor numbers of S1 to S80 also defined

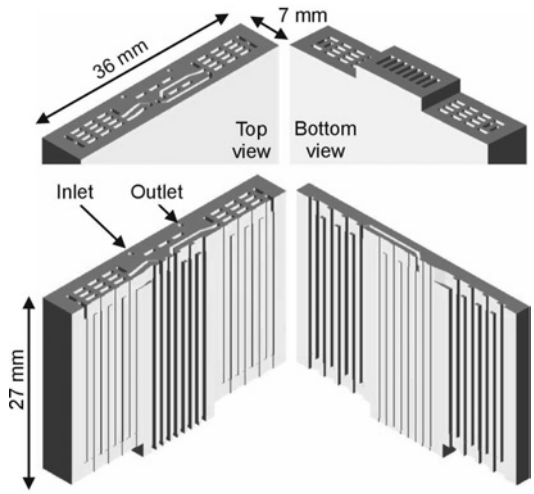

Fig. 4 *CAD drawing of MSL package, dimension 36 mm × 27 mm × 7 mm*

for moving the base (build platform). For each layer, the DMD modulates the light in such a way that the layer mask pattern appears under the resin tray. DMD does this by tilting the mirrors toward or away from the light source. Each layer mask is stored as a mono picture file with each pixel corresponding to a mirror state. Upon exposure, the pattern corresponding to the mask cures the resin. This layer of resin is trapped between the resin tray and the build platform. Once cured, the Z-stage (driven by a lead screw and a stepper motor) moves upwards by the layer thickness step. As the surface of the resin tray is coated with a silicone-based material with lower coefficient of friction than the build platform, the cured layer will detach from the resin tray and stay attached to the build platform. Table 3 gives information on the specification of the MSL system. Typically 25 μm slices were used in the *Z*-direction with a build time of typically 10 s per slice.

A CAD drawing of the microfluidic package, with channel dimensions of 2.4 m × 0.5 mm × 0.5 mm, is shown in Fig. 4. Here the drawing has been cross-sectioned to make the internal channels visible. As can be seen in Fig. 4 the microfluidic package has been designed to contain multiple channels, stacked in the *Y*-direction, with openings and the top and bottom of each channel. The openings in the centre section at the bottom are designed to encompass blocks of 5 sensors, with each sensor within the block having a different sensing layer (i.e. from Fig. 3, one block would be sensors S1, S17, S33, S49 and S65). The remaining openings are there to aid cleaning of any residual resin.

After fabrication the microfluidic package was coated with a retentive layer. Here an evaporation technique using a commercial machine (PDS 2010 Labcoater^{TM} 2 (Specialty Coating Systems, Indianapolis, USA)), was used to deposit Parylene C. This material is very similar to other GC stationary phase materials with the added advantage of room temperature deposition. However, as this material is relatively new as a stationary phase, its retention characteristics have not been fully studied hence the diffusion and partition coefficients of various analytes are not available. Initial investigations show it has similar retention characteristics to PEG [11]. The deposition is performed in a vacuum and took approximately 3½ hours to deposit a 10 μm thick layer.

Once the deposition of Parylene C was completed, the holes on the top and bottom were sealed by placing a strip of plastic (also formed from MSL) over the holes. Uncured resin was used as a sealant, which was then cured in natural light. The package was fitted over the sensor array, again sealed with uncured resin (resin was painted onto the underside of the package and pressed onto the sensor array). Metal pipe fittings were finally added to the micro-package for connection to a vapour flow system. A photograph of the micro-package, after Parylene C coating and after final assembly, is shown in Fig. 5.

Table 3: Build specification of perfactory system

System variant	perfactory mini SXGA (multi lens)
resolution	SXGA: 1280 × 1024 pixel
build envelope XYZ	41 × 33 × 230 mm
pixel size XY	32 μm pixel (16 μm with 1/2 pixel shift)
layer thickness Z	25 μm

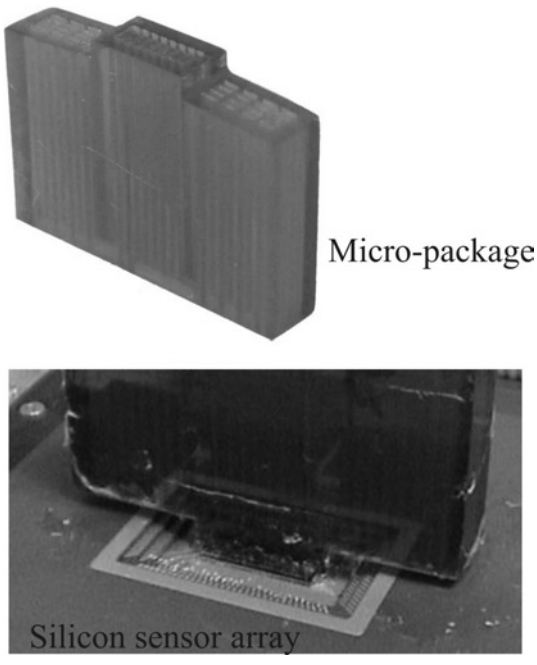

Fig. 5 *Photographs of MSL micro-package and final assembled system*

4 Experimental setup

For testing, the sensor chip was connected to a custom electronic interface where each chemical sensor was used as the feedback resistor of an op-amp (OP2277, Analog Devices) in an inverting configuration. The output voltage was then sampled by on-board 16-bit ADCs (AD7805, Analog Devices) controlled through a National Instruments PC-DIO-96 and LabVIEW™ (version 6.1) control and data storage software. Finally the fluidic package was connected to a custom-made vapour flow system. This system can inject short pulses of simple and complex odours in air over the sensors at different flow rates. Further details of the test setup can be found in [13].

To evaluate our artificial olfactory mucosa, first simple odours of ethanol and toluene vapour in air were injected into the microfluidic system; the temperature was 30 ± 2 °C and relative humidity of $40 \pm 5\%$ throughout all of the experiments. The carrier gas used for all the tests was laboratory air. This was done to keep all the results as close as possible to real life conditions. Ethanol and vapour concentrations were set to 22 and 12 PPT (parts per thousand), respectively, controlled through the use of a cooling bath (Colora, Germany, Model WK141) and used the saturated head space.

Before each experiment, the carrier gas flowed through the system for 1 min to stabilise the sensor resistance. The vapour pulse was introduced at time $t = 1$ s and turned off at time $t = 101$ s to give, for example, a 100 s pulse duration. Each test lasted for 30 mins. Finally, a set of complex odours (milk, cream, a mixture of these at a 50:50 ratio by volume, vanilla, peppermint and a mixture of these 50:50 ratio by volume), were used to evaluate more meaningfully the olfactory capability of the microsystem. For both the simple and complex odours, five repetitions of each experiment were performed. For the complex odours, as before, saturated headspace was used at with a sample temperature of 25 ± 2 °C.

5 Results

Experimental results, taken at a flow rate of 25 and 150 ml/min, show that the retentive layer causes very different delays along the micro-channel of up to 72 and 168 s for ethanol and toluene vapours, respectively. This was calculated by comparing the time the first and last sensors (PCL coated sensors in this case) reached 50% of its maximum response value.

Fig. 6 shows a comparison of sensor responses at different locations along the channel to ethanol and toluene vapours in air. For Fig. 6*a*, both ethanol and toluene vapours pulses reach the sensor at the same time. As the pulses travel along the channel to *b*, the retention effects on the two vapours become significant. Towards the outlet at *c*, the two vapours pulses are partly separated, showing the microsystem is behaving like a basic GC column.

For the complex odours, the responses of 5 sensors (S34 – PEG, S38 – PEG, S57 – PCL, S27 – PEVA and S30 – PSB) placed along the channel were recorded. The spatio-temporal signals for the various odours were analysed by principal components analysis (PCA) to determine the viability to perform linear classification. For simplicity, the spatial signal utilised only the response magnitude (i.e. ΔV, the maximum change in output voltage) and the temporal signal used the time at which the output reached 50% of ΔV. These experiments were conducted at a flow rate of 25 ml/min and pulse width of 25 s with five replicates. Results from the sensor array showed $>5\%$ variation

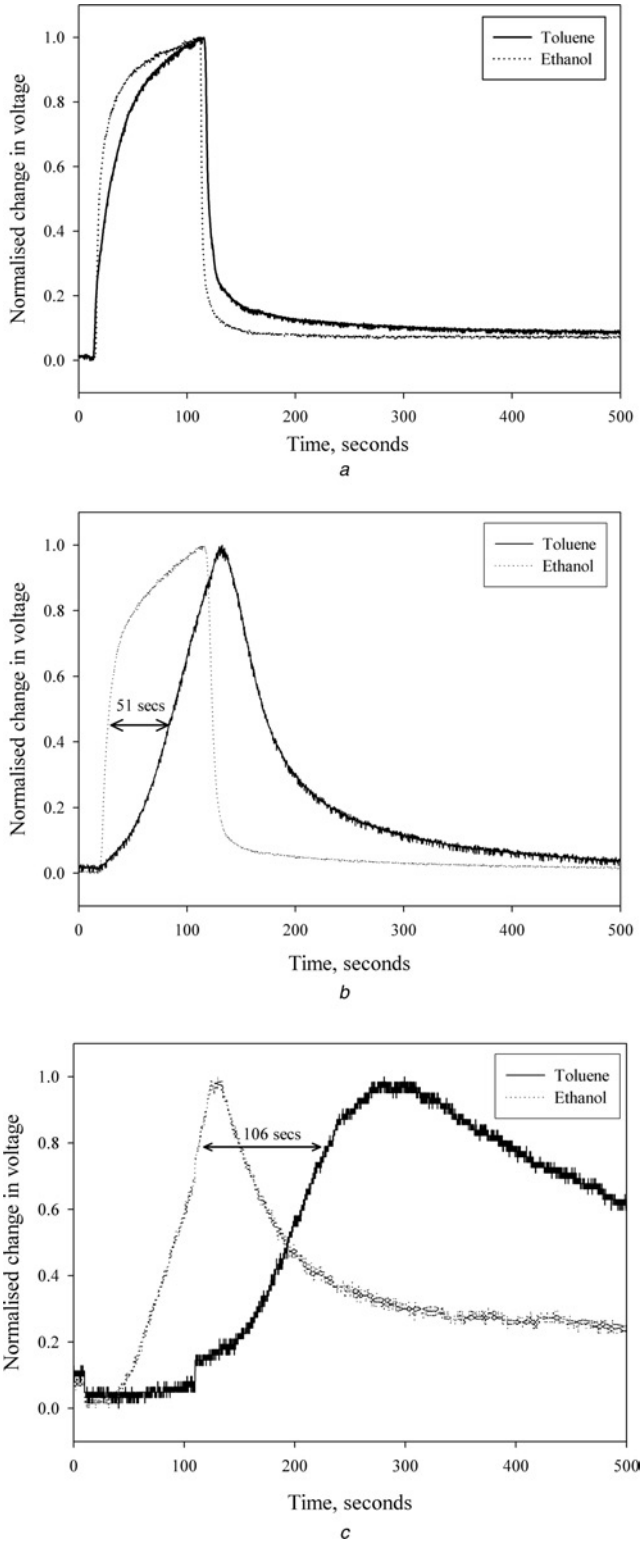

Fig. 6 *Varying temporal signals for simple vapours on microsystem (PEG sensors only)*

a Sensor S50 (25 mm from inlet) response
b Sensor S54 (900 mm from inlet) response
c Sensor S63 (2375 mm from inlet) response (flow rate 25 ml/min)

in either temporal or spatial response between all the tests, as shown in Table 4. Included within Table 4 are the average spatial and temporal values. It can be noted that the spatial sensor response is negative as well as positive. In such cases, it shows that the resistance of the film has reduced. In addition, it can be seen that the temporal values, in some cases, do not increase for sensors placed further along the column. This is due to the different sensing

Table 4: Spatial and temporal values for sensor responses to simple and complex odours

	ethanol	toluene	ethanol + toluene	milk	cream	milk + cream	peppermint	vanilla	vanilla + peppermint
Spatial data (ΔV)									
S34 Av.	0.235	−0.658	0.209	−0.385	−0.423	−0.338	−0.513	−0.474	−0.411
s.d.	0.017	0.054	0.018	0.014	0.016	0.006	0.061	0.026	0.008
S28 Av.	0.303	−1.156	0.264	−0.534	−0.584	−0.462	−0.992	−0.743	−0.705
s.d.	0.016	0.095	0.031	0.037	0.031	0.007	0.133	0.067	0.025
S57 Av.	0.015	0.335	0.014	0.070	0.079	0.056	0.186	0.098	0.104
s.d.	0.002	0.038	0.001	0.005	0.006	0.002	0.010	0.001	0.002
S27 Av.	0.158	3.235	0.152	0.117	0.112	0.109	1.619	0.280	0.586
s.d.	0.011	0.293	0.007	0.010	0.007	0.019	0.079	0.004	0.013
S30 Av.	0.097	1.965	0.089	0.077	0.082	0.069	0.892	0.157	0.324
s.d.	0.005	0.170	0.006	0.008	0.009	0.005	0.036	0.005	0.007
Temporal data (s)									
S34 Av.	169.51	109.22	138.67	110.13	87.04	113.68	80.28	94.18	98.71
s.d.	21.16	0.62	20.33	23.67	7.77	5.10	26.24	4.71	5.29
S28 Av.	181.24	14.79	146.08	103.99	83.80	106.50	29.25	68.14	78.53
s.d.	11.82	1.68	26.09	16.06	7.41	14.29	3.92	17.94	10.78
S57 Av.	207.19	25.06	196.48	66.22	47.93	78.48	31.54	42.63	51.14
s.d.	11.75	3.40	4.59	2.71	2.99	1.23	3.23	1.92	1.22
S27 Av.	231.2	29.89	236.69	32.08	18.59	38.86	57.76	51.39	67.51
s.d.	16.26	0.84	8.61	4.86	1.17	10.20	2.31	25.13	2.38
S30 Av.	262.71	54.77	251.93	74.68	65.00	93.46	112.49	95.70	113.51
s.d.	17.61	1.24	18.70	17.91	9.30	9.61	2.74	1.52	1.80

layers, which are used in Table 4, having both different response times and are responding to different chemical components within the odour pulse. Three PCAs were performed, one operated on the spatial data only, a second used the temporal data, whereas the third utilised the combined data (spatio-temporal data). Fig. 7 shows the results of the combined data analysis, clearly showing that the test odours can be linearly separated.

It was observed that the distance between the complex odours, as represented in multivariate vector space, was greater for the spatio–temporal data than that for the spatial data or temporal data alone. The performance of the spatial data (used in a conventional e-nose) was also found to outperform that of the temporal data alone. Care must be taken when analysing the different datasets because of the doubling in the dimensionality of the spatio–temporal dataset and magnitude of signals. A more detailed parametric study of the responses is being carried out using both linear and non-linear classification methods, such as discriminant and radial basis function analyses. The results of this study will be published subsequently.

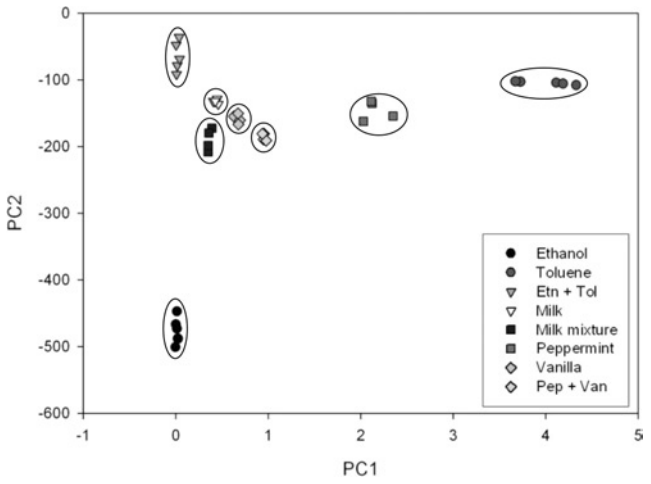

Fig. 7 *PCA plots with spatio–temporal data of five sensors [(S34 (PEG sensor 30 mm from inlet), S38 (PEG sensor 1060 mm from inlet), S57 (PCL sensor 2100 mm from inlet), S27 (PEVA sensor, 2160 mm from inlet), and S30 (PEVA sensor, 2200 mm from inlet)]*

6 Conclusions

Here we report on the first attempt to make an artificial olfactory mucosa by combining a silicon sensor array with a microfluidic package. This system has been designed and fabricated to exploit the nasal chromatographic phenomena, which has been observed in the mammalian olfactory system. Our system aims to replicate this biological process by generating similar spatio–temporal signals. Here an 80 element microsensor array, with five different sensor tunings, has been combined with a 2.4 m long Parylene C coated channel fabricated using MSL. The distributed microsensor system was tested with both simple and complex odours to determine its ability to generate both spatial and temporal signals. The results show that the ‘e-mucosa’ system can produce useful spatio–temporal signals for both types of odours, with a temporal delay of up to 106 s. Though these response times are still considerable longer than the biological system, we believe that future systems with improved micro-mucosa, incorporating smaller channels and faster sensors will result in a biomimmetic system, which more closely matches the performance of the biological olfactory system and could well be the critical factor in improving existing e-nose instruments.

7 Acknowledgment

We would like to thank EPSRC (grant no. GR/R37975/01) for funding this research project.

8 References

1 Goldstein, E.B.: 'Sensation and perception, Sixth Edition' (Wadsworth Inc Fulfilment, 2000, 2nd edn.)
2 Buck, L., and Axel, R.: 'A novel multigene family may encode odorant receptors: a molecular basis for odor recognition', *Cell*, 1991, **65**, pp. 175–187
3 Gardner, J.W., and Bartlett, P.N.: 'Electronic noses: principles and applications' (Oxford University Press, Oxford, 1999, 1st edn.)
4 Mozell, M.M., Sheehe, P.R., Hornung, D.E., Kent, P.F., Youngentob, S.L., and Murphy, S.J.: '"Imposed" and "inherent" mucosal activity patterns. Their composite representation of olfactory stimuli', *J. Gen. Physiol.*, 1987, **90**, (5), pp. 625–650
5 Kent, P.F., Mozell, M.M., Youngentob, S.L., and Yurco, P.: 'Mucosal activity patterns as a basis for olfactory discrimination: comparing behavior and optical recordings', *Brain Res.*, 2003, **15, 981**, (1–2), pp. 1–11
6 Kent, P.F., Mozell, M.M., Murphy, S.J., and Hornung, D.E.: 'The interaction of imposed and inherent olfactory mucosal activity patterns and their composite representation in a mammalian species using voltage-sensitive dyes', *J. Neurosci.*, 1996, **16**, (1), pp. 345–353
7 Quenet, E.B., Horn, D., and Dreyfus, G.: 'Temporal coding in an olfactory oscillatory model', *Neurocomputing*, 2001, **38**, (40), pp. 831–836
8 Lysetskiy, M., Lozowski, A., and Zurada, J.M.: 'Invariant recognition of spatio-temporal in the olfactory system model', *Neural Process. Lett.*, 2002, **15**, pp. 225–234
9 Tan, S.L., Covington, J.A., and Gardner, J.W.: 'Velocity-optimised diffusion for ultra-fast polymer-based resistive gas sensors', *IEE Proc. Sci. Meas. Technol.*, 2006, **153**, (3), pp. 94–100
10 Matthews, B., Li, J., Sunshine, S., Lerner, L., and Judy, J.W.: 'Effects of electrode configuration on polymer carbon-black composite chemical vapour sensor performance', *IEEE Sensor J.*, 2002, **2**, pp. 160–168
11 Noh, H.S., Hesketh, P.J., and Frye-Mason, G.C.: 'Parylene gas chromatographic column for rapid thermal cycling', *J. Microelectromech. Systems*, 2002, **11**, (6), pp. 718–725
12 Tan, S.L., Covington, J.A., and Gardner, J.W.: 'Ultrafast chemical-sensing microsystem employing resistive nanomaterials', *Proc. SPIE*, 2004, **5389**, pp. 366–376
13 Tan, S.L.: 'Smart chemical sensing microsystem: towards a nose-on-a-chip'. PhD thesis, School of Engineering, University of Warwick, Coventry, UK, September 2005